Epidermal Impedance Sensing Sheets for Precision Hydration Assessment and Spatial Mapping

Xian Huang, Huanyu Cheng, Kaile Chen, Yilin Zhang, Yihui Zhang, Yuhao Liu, Chenqi Zhu, Shao-chi Ouyang, Gil-Woo Kong, Cunjiang Yu, Yonggang Huang, and John A. Rogers*

***Abstract*—This paper presents a class of hydration monitor that uses ultrathin, stretchable sheets with arrays of embedded impedance sensors for precise measurement and spatially multiplexed mapping. The devices contain miniaturized capacitive electrodes arranged in a matrix format, capable of integration with skin in a conformal, intimate manner due to the overall skin-like physical properties. These "epidermal" systems noninvasively quantify regional variations in skin hydration, at uniform or variable skin depths. Experimental results demonstrate that the devices possess excellent uniformity, with favorable precision and accuracy. Theoretical models capture the underlying physics of the measurement and enable quantitative interpretation of the experimental results. These devices are appealing for applications ranging from skin care and dermatology, to cosmetology and health/wellness monitoring, with the additional potential for combined use with other classes of sensors for comprehensive, quantitative physiological assessment via the skin.**

***Index Terms*—Depth profiling, epidermal electronics, hydration sensing, multiplexing, spatial mapping.**

I. Introduction

HUMAN skin is composed of complex structures in which water influences synthetic pathways for lipids [1] and DNA [2], and defines mechanical characteristics [3] and electrical properties [4], as well as the overall appearance and surface texture [5]. Decreases in skin hydration levels can lead to eczema, acne, itching, and cracking of the stratum corneum (SC), all of which can increase skin roughness and compromise its ability to prevent transdermal water loss (TEWL). Accurately measuring hydration levels of the skin can, therefore, be important in dermatology and cosmetology as a means for analyzing various disease states (e.g., eczema, psoriasis, atopic dermatitis, and ichthyosis) [6]–[9] and assessing factors (e.g., environmental, age, stress, and hormone) [10]–[13] that can be associated with abnormal skin responses. Hydration can also determine the effectiveness of medical therapies [9], [14]–[16], and cosmetic treatments [17]–[20].

Skin hydration levels are typically characterized by measurements of electrical impedance [4], [21], [22], thermal conductivity [23], spectroscopic properties [24]–[26], and mechanical characteristics [27], [28]. Impedance, however, represents one of the most direct indications, due to the strong influence of water content on conductivity and permittivity of the skin. Instrumental simplicity, low cost, and minimally invasive operation with commercially available tools existing in both single point [29]–[32] and multipoint mapping [33]–[35] formats provide further advantages over other measurement methods. The precision of the measurement, however, depends critically on the effectiveness of contact between the soft, curved, and textured surface of the skin and the rigid, planar metal electrodes that are typically used [29]. As a result, such devices often incorporate pressure sensors to facilitate application of specific, repeatable levels contact force during measurements [29]. Such sensors help minimize, but do not eliminate, problems in irreproducibility that arise from uncontrolled variations in contact properties [36], thereby resulting in random fluctuations in the device output. Furthermore, redistribution of water within the SC as a consequence of mechanical stress of compression forces on the skin surface tends to alter the skin hydration [37]–[39], and thus affects the accuracy of hydration measurement.

We recently reported a hydration sensor technology based on differential impedance measurements using a soft, conformal system designed to offer mechanical properties well matched to the epidermis itself [40]. This class of "epidermal" sensor enables spontaneous contact with the skin, driven by van der Waals forces alone, without application of pressure, thereby leading to precise, completely noninvasive hydration determination, with minimized common-mode disturbances. One limitation of our previously described sensor is that, as with commercially available meters, hydration levels are measured only in a single, confined area, due to the small number of sensing electrodes. A concept for a epidermal device capable of hydration mapping was recently described [40]. This work builds on those ideas and provides systematic experimental and theoretical studies of

Manuscript received March 3, 2013; revised April 12, 2013; accepted May 17, 2013. Date of publication May 31, 2013; date of current version September 14, 2013. This work was supported in part by the U.S. Department of Energy under Grant DE-FG02-07ER46453 and Grant DE-FG02-07ER46471. The work of J. A. Rogers was supported by the National Security Science and Engineering Faculty Fellowship. *Asterisk indicates corresponding author.*

X. Huang, K. Chen, Y. Zhang, Y. Liu, C. Zhu, S.-C. Ouyang, G.-W. Kong, and C. Yu are with the Frederick Seitz Materials Research Laboratory, University of Illinois at Urbana-Champaign, Urbana, IL 61801 USA (e-mail: xh2123@illinois.edu; chen95@illinois.edu; zhang163@illinois.edu; liu104@illinois.edu; zhu47@illinois.edu; ouyang4@illinois.edu; kong7@illinois.edu; yu.cunjiang@gmail.com).

H. Cheng and Y. Huang are with the Department of Mechanical Engineering, Northwestern University, Evanston, IL 60208 USA (e-mail: huanyucheng2014@u.northwestern.edu;y-huang@northwestern.edu).

Y. Zhang is with the Northwestern University, Mechanical Engineering, Evanston, IL 60208 USA, and also with Center for Mechanics and Materials, Tsinghua University, Beijing 100082, China (e-mail: yihui.zhang@northwestern.edu).

*J. A. Rogers is with the Frederick Seitz Materials Research Laboratory, University of Illinois at Urbana-Champaign, Urbana, IL 61801 USA (e-mail: jrogers@illinois.edu).

Color versions of one or more of the figures in this paper are available online at http://ieeexplore.ieee.org.

Digital Object Identifier 10.1109/TBME.2013.2264879

all essential aspects of device operation. The resulting systems noninvasively quantify regional variations in skin hydration, at uniform or variable skin depths, in modes that are mechanically invisible to user, due to the epidermal physical properties of the devices. In addition, we report theoretical models, supported by systematic experimental data that can account for the underlying physics of the measurement, and also aid in quantitative interpretation of the results. The results demonstrate highly uniform device response with irregularities that primarily reflect the skin variations. The collective sensor output can be used for continuous hydration imaging with characteristic measurement depths defined by the frequency and the geometry of the electrodes [41]–[43]. Choices of design parameters of the array, such as the electrode sizes, spacings, and numbers of pairs of electrodes, define the spatial resolution. With modest effort, spatial coverage of the device can be further expanded while maintaining conformal skin attachment with maximized sensitivity to skin impedance. These attributes suggest that this type of technology, particularly when combined with other classes of sensors in a single system, can be integrated intimately with the epidermis, providing valuable, wide-ranging applications in human healthcare and wellness evaluation via quantitative measurements through the skin.

II. Principle and Sensor Design

Hydration mapping is conducted directly on the skin using multiplexing impedance measurements with epidermal devices. Similarity in measurement principles of epidermal devices and commercial hydration sensors (CHS) allows direct conversion of measured skin impedance to hydration level provided by the CHS. In particular, both the conductivity and permittivity of the skin change with hydration levels due to primarily variations in the electrical contributions from free and bound water in the skin [44]. Individually isolated capacitive electrodes allow multiplexed operation with relatively simple measurement systems.

A. Epidermal Impedance Sensors for Spatial Hydration Mapping

Fig. 1 shows images and schematic illustrations of an epidermal skin hydration mapping sensor that consists of 64 channels of planar electrode pairs designed to quantify skin impedance across an area of 15×15 mm^2. Each pair of electrodes includes an inner circular disk and an outer annulus, equally distributed across the overall area of the device, in an 8×8 array format. Circular electrodes in a given row act as current sources that share a common current supply; annulus electrodes in a given column provide current sinks that are connected in series. As a result, any electrode pair can be individually selected for impedance measurement. Fig. 1(f) provides a cross-sectional illustration of two adjacent electrodes that form direct contacts to the skin. The associated electrical field penetrates the skin but is mostly confined within the SC region, for the electrode geometries and frequencies of applied current explored here. Devices used for measuring skin hydration over large areas with uniform or different skin depths (by use of different geometries and/or

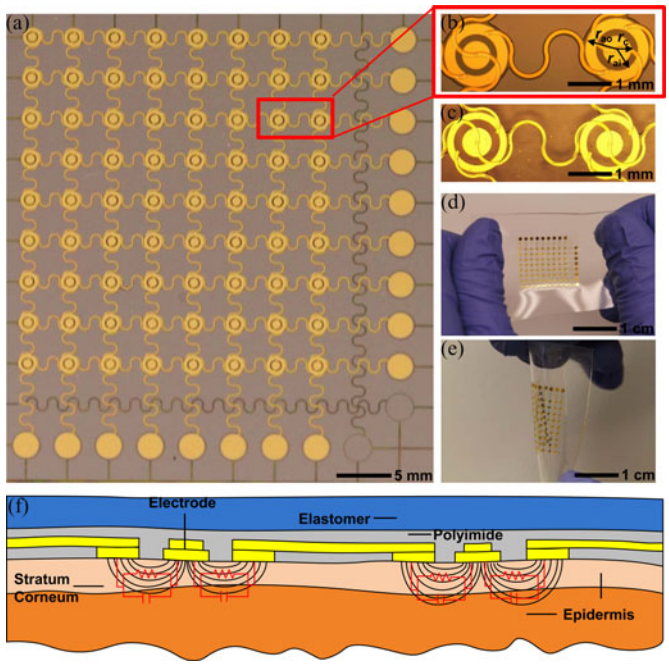

Fig. 1. (a) Optical micrograph of an epidermal hydration mapping system. (b) Representative pair of sensors, showing central circular electrode pads with radii r_{c} and surrounding concentric ring electrodes with inner and outer radii (r_{ai} and r_{ao}). (c) Two electrodes on a hydration depth-profiling sensor with different r_{c} to allow measurement at a different skin depth. (d) A fabricated device under a stretching deformation. (e) A fabricated device under bending and twisting. (f) Diagram of skin integration and measurement principle.

frequencies, as described subsequently) adopt similar designs and are referred to as epidermal hydration mapping sensors and depth profiling sensors, respectively. In particular, inner circular electrodes have fixed radii r_{c} throughout the mapping array [see Fig. 1(b)], while radii of the circular electrodes on the depth profiling sensors are varied between rows to alter the distribution of electrical field within the skin [see Fig. 1(c)]. The device configured for depth profiling does so across the area of the array, where different electrode pairs measure to different characteristic depths. Depth profiling at a single location, with a single electrode pair, can be achieved by scanning the measurement frequency. The electrodes terminate at circular bonding pads aligned vertically and horizontally near the edge of the overall system, and are joined through serpentine interconnects in mesh layouts. The latter design feature provides epidermal mechanics when the system is implemented on soft, thin elastomeric substrates. Physical isolation between inner and outer electrodes allows each pair in the array to be individually selected with minimal crosstalk, for mapping in a simple, multiplexed mode.

The fabrication processes are similar to those recently reported for related devices [40]. Briefly, a sacrificial layer of polymethylmethacrylate (PMMA; 500 nm thick) and a layer of polyimide (PI; 1 μm thick) are spin-cast onto a silicon (Si) wafer [see Fig. 2(a)]. Serpentine interconnect traces consist of photolithographically patterned bilayers of Cr (5 nm) and Au (400 nm). A subsequent coating of PI (1 μm) [see Fig. 2(b)] electrically insulates the top surfaces. Selected regions of PI are removed by reactive ion etching (RIE) to form via contacts

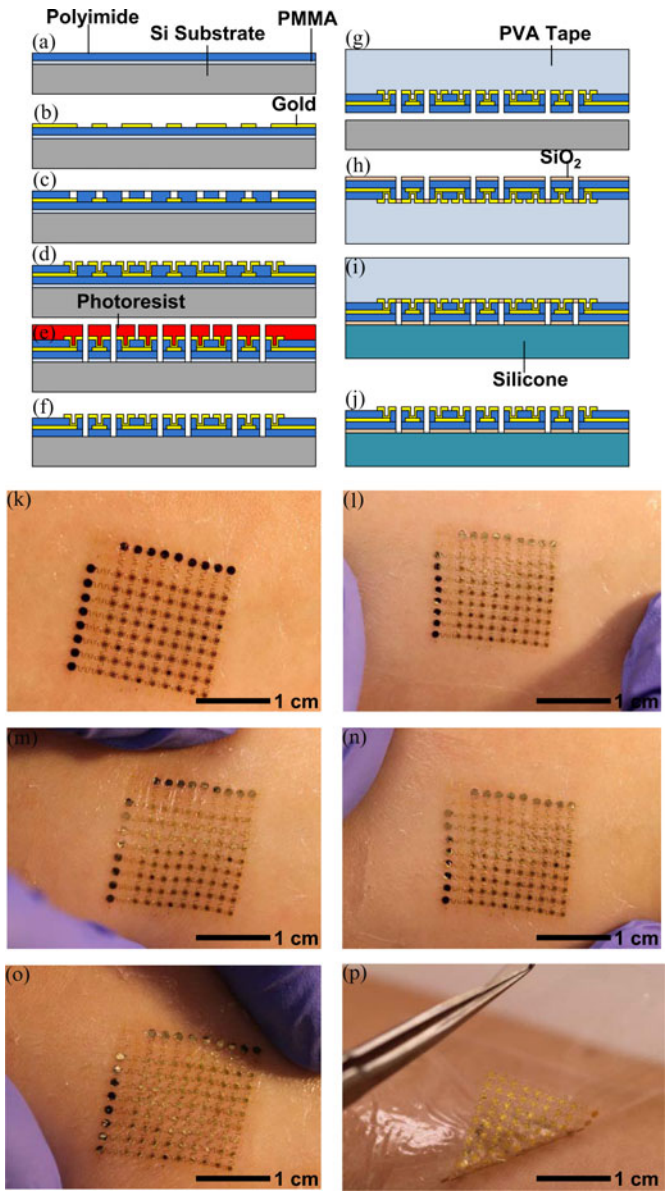

Fig. 2. (a) to (j) Schematic illustration of steps for fabricating epidermal hydration sensors. (k) to (p) Epidermal hydration sensor mounted on the skin of the forearm. This sequence of images shows the device, undeformed (k), and uniaxially stretched along the horizontal (l), vertical (m), diagonal right (n), and diagonal left (o) directions. Here, the device adheres to the skin by van der Waals interactions alone, thereby allowing it to be easily peeled from the skin using tweezers (p).

[see Fig. 2(c)]. An additional patterned bilayer of Cr/Au (5 nm/200 nm) forms the electrodes [see Fig. 2(d)]. Patterned etching through entire stacked layers by RIE defines the open mesh layout [see Fig. 2(f)]. Eliminating the sacrificial PMMA layer by immersion in acetone for 5 min at 100° C enables removal of the device with a water-soluble poly(vinyl alcohol) (PVA) tape (Wave Solder Tape 5414, 3M Company) (see Fig. 2(g)]. Layers of Ti/SiO_2 (5/40 nm) [see Fig. 2(h)] deposited onto the backside allows chemical bonding to a thin, low-modulus silicone substrate (Solaris, Smooth-On, Inc.) [see Fig. 2(i)]. Finally, the PVA tape on the device is removed by water [see Fig. 2(j)], to yield an integrated device with excellent stretchability [see Fig. 1(d)] and flexibility [see Fig. 1(e)].

B. Conformal Contact of Epidermal Hydration Sensors to the Skin

The epidermal hydration mapping sensors can be integrated onto the skin using a previously introduced physical lamination process followed by rinsing in water to remove the temporary carrier substrate [45] resulting in intimate and conformal skin contact (see Fig. 2(k)]. Devices mounted in this way exhibit excellent compliance and ability to follow skin motions without constraint or delamination (see Fig. 2(i)–(o)]. Devices with comparatively thicker silicone substrates (e.g., 50 to 100 μm) provide sufficient mechanical toughness, and only slightly compromised mechanics, to allow repeated measurements by removing and reattaching to the skin [see Fig. 2(p)]. These reusable devices are fixed at one corner with a small piece of surgical tape, which also partially attaches to the skin. The tape facilitates device handling and improves the consistency of the measurement.

III. Experimental Setup and Methods

A. Epidermal Impedance Sensors for Spatial Hydration Mapping

The circular electrodes in mapping sensors for uniform skin depths involve concentric designs [see Fig. 1(b)], consisting of inner disks (r_c) (200 μm in radius) surrounded by rings (inner radius r_{ai}: 300 μm, outer radius r_{ao}: 450 μm). For sensors designed for various skin depths, r_c increases from 60 to 200 μm with a step of 20 μm across the array, while r_{ai} and r_{ao} are fixed at 300 and 400 μm, respectively [see Fig. 1(c)]. In both of these two cases, each electrode pair is 2 mm away from its nearest neighbors. The electrodes connect to corresponding bonding pads (diameter: 1.2 mm, spacing: 2 mm) through serpentine traces (width 55 μm; $\sim$225 μm radii of curvature). The circular geometries of the electrodes offer symmetries that facilitate theoretical analysis. Similar layouts are common in the types of conventional, rigid macroscale electrodes found in CHS [29], [30].

B. Multiplexing Impedance Analyzer for Hydration Measurement

An LCR meter (E4980 A, Agilent Technologies) equipped with multiplexing measurement capability serves as a system for quantifying the response of the sensors [see Fig. 3(a) and (b)]. Here, the meter sequentially provides an ac voltage $(V_{in}$; 2 V peak to peak) at frequencies between 20 Hz and 2 MHz to each channel [A1 to A8; labeled horizontally from right to left in Fig. 3(b)] of the hydration sensor through a row scanning multiplexer (multiplexer1, ADG 708, Analog Devices). The output voltage V_{out} of each channel [B1 to B8; labeled vertically from top to bottom in Fig. 3(b)] is scanned by the meter with a column multiplexer (multiplexer2, ADG 708, Analog Devices). A computer controlled I/O card (USB-8451, National Instruments) selects pins (a1 to a3, b1 to b3) in the multiplexers that correspond to channels A1 through A8 and B1 through B8. These channels

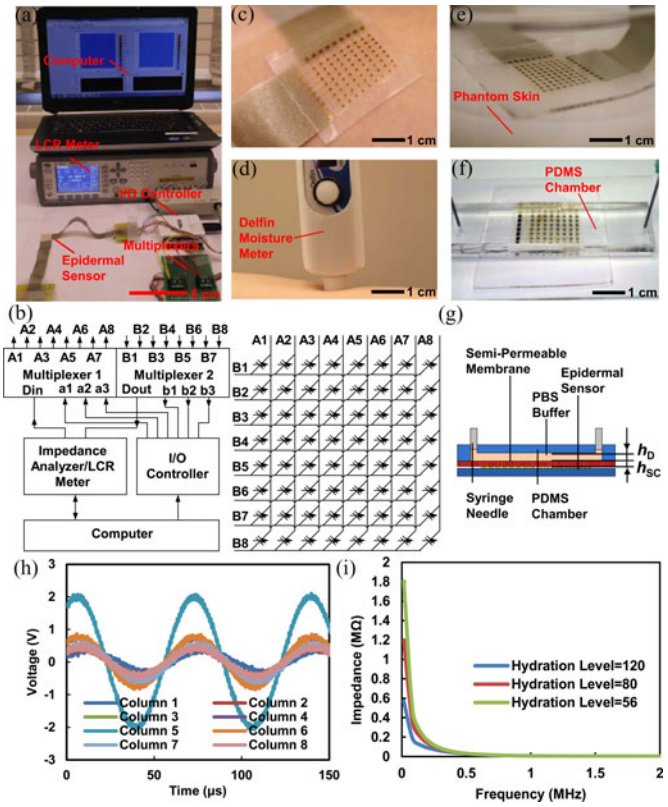

Fig. 3. (a) Image and (b) diagram of the hydration measurement setup, with multiplexed acquisition. (c) and (d) Images of use of an epidermal hydration sensor and a commercial hydration sensor. (e) Application of an epidermal sensor on a phantom skin model for *in vitro* characterization of sensor response. (f) Image and (g) diagram of a microfluidic device for determining the measurement depth of the sensor. (h) Voltage distribution among different columns on an epidermal sensor. Here, column 5 provides a current injection channel. Voltage presented on other columns arises from capacitive coupling of ac signals between columns. (i) Frequency response of a representative epidermal sensor at various hydration levels.

are physically isolated, but capacitively coupled. At any given time, only one row and one column are selected by the multiplexers. Thus, the impedance analyzer measures only the impedance associated with the electrode pair that lies at the crossing point defined by the selected row and the column. Other electrode pairs are electrically isolated from the impedance analyzer by the multiplexers. The *LCR* meter converts the corresponding $V_{\rm out}$ to an impedance value by comparing the amplitude and the phase of $V_{\rm out}$ to $V_{\rm in}$, while preventing significant capacitive coupling to neighboring channels [see Fig. 3(h)]. Repeated row scanning followed by column scanning allows individual addressing of all of the electrode pairs in the device. The collected impedance values can be combined to yield spatial maps.

C. Experimental Methods and Materials

Experimental evaluations involve *in vitro* and *in vivo* testing. Both the magnitude and phase of the sensor impedance can be used to quantify skin hydration [40]. However, only the impedance magnitude is presented, to reflect the collective effects of changes in skin conductivity and permittivity due to hydration variations [46]–[48]. *In vitro* studies use a thickness-controlled microfluidic setup to evaluate the dependence of the effective measurement depth, defined by the depth beyond which the sensor impedance ceases to increase, on electrode geometry and sensing frequency [41]–[43]. The uniformity of the sensor response is characterized in air and on a phantom skin sample [49], [50] made of a combination of water, agar, polyethylene, sodium chloride, sodium azide, and TX 151 (Oil Center Research). The agar provides a solid matrix; polyethylene and sodium chloride set the permittivity and conductivity; sodium azide is used as a preservative. The addition of TX-151 alters the mechanical properties of the phantom skin, resulting in a gelatin-based material that can be molded to form a planar surface with hydration levels and electrical properties comparable to the human skin. The thickness-controlled microfluidic setup and the phantom skin serve to characterize different aspects of device operation: depth profiling and uniformity in response. The platforms either have stacked layers or electrical properties similar to skin. These structures are not, of course, complete skin replicas with similar detailed properties, which leads to some limitations in their use.

In vivo studies are conducted by attaching epidermal hydration mapping sensors to the skin of the ventral forearm and then measuring impedance changes associated with hydration levels across the array at sweeping or fixed frequencies. The epidermal sensors can be easily removed from the skin upon the completion of array scanning to avoid accumulation of water vapor underneath the device from TEWL, which can otherwise decrease the skin impedance. Repeated measurements without removal are less instructive due to such effects, as reported in evaluations using other technologies [30], [51], [52]. Sweeping the frequency of the applied voltage reveals the frequency-dependent impedance changes associated with hydration levels across the array. Hydration measurements are typically conducted at frequencies with maximum observed sensitivity, based on *in vitro* control experiments using the microfluidic setup. With *in vivo* demonstrations, patterns of hydration manually defined on the skin by local application of moisturizing lotions (Intensive Rescue Moisture Body Lotion, Vaseline, Inc.) are revealed by hydration mapping with arrayed sensors. Measurement results are quantitatively converted to hydration levels by calibration against a CHS (MoistureMeterSC Compact, Delfin, Inc.) [29], which measures skin impedance at an excitation frequency of 1.25 MHz and is widely considered as a reliable tool for skin hydration assessment [12], [29], [53], [54].

IV. Results and Discussion

A. In Vitro Characterization of Depth Profiling Sensors

Systematic studies reveal the dependence of the measured impedance on frequency and geometry. Test structures that consist of molded PDMS with microfluidic chambers whose heights $h_{\rm D}$ varies from 10 to 60 μm [see Fig. 3(f) and (g)] provide a platform to approximate, in a rough sense, the structure of human skin. Semipermeable cellulose membranes (Spectra/Por Dialysis Membrane, Spectrum Laboratories, Inc.) with thicknesses ($h_{\rm SC}$) of $\sim$20 μm seal the chambers, to prevent leaking of phosphate buffered saline solutions introduced through

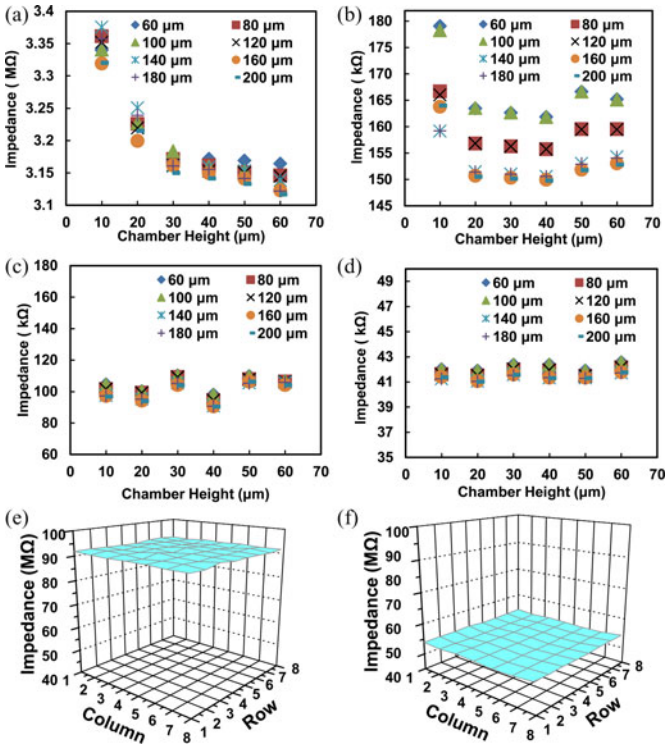

Fig. 4. Changes in impedance as a function of microfluidic chamber height at a frequency of (a) 15 kHz, (b) 250 kHz, (c) 500 kHz, and (d) 1.25 MHz with inner electrode radii changed from 60 to 200 μm. *In vitro* impedance mapping using an epidermal hydration sensor (e) in air and (f) on a phantom skin sample, both recorded at 15 kHz.

inlets/outlets at the periphery. The resulting overall chamber heights $(h_{\mathrm{D}} + h_{\mathrm{SC}})$ are then varied from 30 to 80 μm. Depth profiling hydration sensors that exploit different electrode radii attach to the cellulose membrane. Measurements of the impedance using various sensor geometries for different chamber heights reveal the effective depth of hydration assessment. As shown in Fig. 4(a)–(d), the electrodes respond to the changes of chamber heights differently. The dependence on height is determined by the measurement frequencies and the electrode radii, with the former representing the dominant effect for the systems explored here. For example, at a frequency of 15 kHz, all electrodes exhibit decreasing impedance with h_{D} up to 40 μm [see Fig. 4(a)]. When including the h_{SC}, the effective measurement depth corresponds to a value greater than 60 μm. This depth decreases quickly with frequency. At 250 kHz, most electrodes show impedances that cease to depend on h_{D} greater than 20 μm, equivalent to a 40 μm effective measurement depth [see Fig. 4(b)]. The impedance shows no appreciable change with height at frequencies of 500 kHz and 1.25 MHz, indicating an effective measurement depth less than 20 μm.

The influence of the electrode radii is most prominent at low frequencies. For example, at 15 kHz, the impedance associated with electrodes that have radii r_{c} of 80 μm show height independent responses for heights above 35 μm. Electrodes with r_{c} of 200 μm exhibit impedances that decrease steadily up to heights of 60 μm. This observation indicates that increasing the radii of the inner electrodes while fixing the radii of outer annulus electrodes increases the effective measurement depth. These *in vitro* depth profiling results demonstrate the ability to define measurement depths by suitable selection of measurement frequency and electrode spacing.

B. In Vitro Characterization of Sensor Uniformity

Measurements of the impedance of individual sensors in air and on planar phantom skin samples define the uniformity of the responses [see Fig. 3(e)]. As is evident from the data of Fig. 4(e) and (f), the hydration mapping sensor shows highly uniform behavior. When the sensor is exposed to air, the average impedance of the sensors is ~91.6 MΩ with a standard deviation of 0.3 MΩ, or 0.36%. While on the phantom skin, the average impedance reduces to 274.9 kΩ with variations within 1%. These levels of uniformity exceed those observed in later evaluations on real skin, suggesting that the influence from the skin contours and the intrinsic nonuniformities in hydration across the measured regions of the skin [55], [56] contribute in a significant way to observed variations of impedance among electrodes. In addition, the variation (0.36%) of electrode impedance in air indicates minor inconsistencies introduced during the fabrication processes and potentially within the experimental setup. The uniformity of the hydration sensors can be further improved by applying reference detection and optimizing the fabrication processes as well as the experimental setup.

C. In Vivo Frequency Dependence of Impedance

The amplitude of the impedance measured at each of the sensor channels changes monotonically with the level of skin hydration, throughout the RF range from 15 kHz to 2 MHz. Representative responses of a single sensor channel appear in Fig. 3(i). As the hydration level changes from 56 to 120 (arbitrary units from the CHS), the impedance amplitude decreases from 1.81 to 0.57 MΩ at 15 kHz and from 2.25 to 2.02 kΩ at 2 MHz. Furthermore, at a fixed hydration level of 80, the impedance amplitude decreases with increasing frequency, from 1.2 MΩ at 15 kHz to 2.15 kΩ at 2 MHz. These trends on the skin coincide with the reported dielectric behavior of aqueous electrolyte solutions [57]–[60], in which electrical conductivity is relatively stable throughout the measured frequency range, while the permittivity decreases with increasing frequency until the frequency reaches that characteristic of the dipolar polarization time. The results also indicate that changes in impedance with hydration are most substantial at low measurement frequencies (e.g., 15 kHz) where the capacitive components of the complex impedance are large. Decreased sensor impedance at higher hydration levels can be attributed to an increase in electrical skin conductivity and permittivity [32], [44]. Water molecules in the skin create ionic pathways for charge transport, increase the density of dipoles, and improve the flexibility of keratin in the SC, all of which leads to enhanced ability of the skin to store electrical energy and respond more readily to applied electrical fields [61].

Fig. 5(a)–(d) show changes in impedance with hydration at frequencies of 15 kHz and 1.25 MHz, for all sensor channels. As the hydration increases, the conductivity and permittivity of the

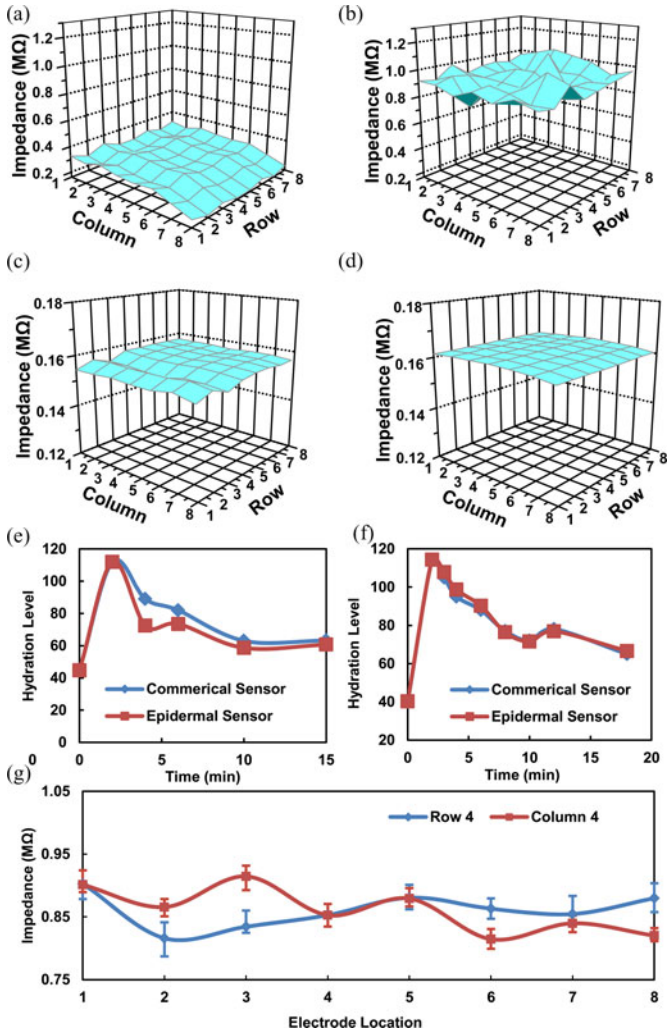

Fig. 5. Hydration map recorded with an epidermal sensor at a measurement frequency of 15 kHz, for skin with known hydration level between (a) 112 and (b) 45. A different measurement with similar map for skin with known hydration levels of (c) 114 and (d) 40 recorded at 1.25 MHz, calibrated hydration levels recorded with selected electrodes in an epidermal sensor at (e) 15 kHz and (f) 1.25 MHz, with comparison to results from a commercial sensor. (g) Impedance variation of all electrode pairs on row 4 and column 4 of the epidermal sensor at a constant hydration level of 45 and a frequency of 15 kHz of six repeated measurements.

skin both increase, leading to a decrease in the real (resistive) and imaginary (capacitive) parts of the complex impedance. The result is a monotonic decrease of skin impedance. The magnitude of the change in impedance diminishes with increasing frequency. For example, the impedance decreases by 71.1% and 5.4% at 15 kHz and 1.25 MHz, respectively, when the hydration level increases from 40 to 114. These observations suggest that the sensitivity is best at low frequencies (e.g., 15 kHz) for the range examined. The impedance values measured from individual channels vary by 5% across the array, indicating good uniformity in sensor response. As shown subsequently through *in vitro* measurements on phantom skin samples and in air, these variations mostly arise from skin contours underneath the sensor and intrinsic variations in hydration over the measured regions of the skin, with additional effects of slight variations associated with the fabrication processes. The data indicate that impedance values can be converted into hydration levels using a simple linear relationship [40], whose coefficients can be calculated using two reference hydration levels and the corresponding impedance values (amplitude and/or phase). The converted results shown in Fig. 5(e) and (f) exhibit excellent agreement with the CHS. Results of six repeated measurements obtained by removing the device and reattaching it to the skin are consistent and vary within ~3% [see Fig. 5(g)]. These changes are much smaller than those associated with observed variations in hydration [up to ~70%, in Fig. 5(a) and (b)].

D. Modeling Results

Analytical study can be used to reveal the frequency and geometry dependence of electrode impedance. Each stacked skin layer can be equivalent to a parallel *RC* circuit with capacitance C and resistance R, both of which can be obtained from the electric field in the skin. The electric potential φ in an electrical field formed by a concentric pair of circular electrodes can be written as

$$\frac{\partial^2\varphi}{\partial r^2}+\frac{1}{r}\frac{\partial\varphi}{\partial r}+\frac{\partial^2\varphi}{\partial z^2}=0 \tag{1}$$

where r is the radial distance from the central axis of electrodes and z is the depth from the electrode/skin interface. As a result, the electric potentials on inner circular and the outer annulus electrodes can be obtained through Hankel transform [62], resulting in the determination of the potential difference $\Delta\varphi$ between the electrodes, as well as the charge Q on each electrode in a form

$$Q=-2\pi\varepsilon\int_0^{r_1}\frac{\partial\varphi}{\partial z}|_{z=0,0<r<r_1}\,r\,dr \tag{2}$$

which in turn determines the capacitance C as $C=Q/\Delta\varphi$. The resistance can be approximately related to the capacitance by $R\sigma_{\rm SC}=\varepsilon_{\rm SC}/(C)=L/A$, where $\sigma_{\rm SC}$ is the conductivity of stratum corneum, L the effective length of the dielectric material layers, and A the area of electrodes. Thus, the impedance of the electrodes can be obtained as

$$|Z|=\frac{2}{\pi\varepsilon_{\rm SC}\sqrt{\frac{\sigma_{\rm SC}^2}{\varepsilon_{\rm SC}^2}+4\pi^2f^2}}\cdot\int_0^\infty\left\{\frac{1}{\xi^2}\left[\frac{J_1(\xi r_{\rm c})}{r_{\rm c}}-\frac{r_{\rm ao}J_1(\xi r_{\rm ao})-r_{\rm ai}J_1(\xi r_{\rm ai})}{r_{\rm ao}^2-r_{\rm ai}^2}\right]^2\cdot\frac{\varepsilon_{\rm D}\tanh(\xi h_{\rm SC})\tanh(\xi h_{\rm D})+\varepsilon_{\rm SC}}{\varepsilon_{\rm D}\tanh(\xi h_D)+\varepsilon_{\rm SC}\tanh(\xi h_{\rm SC})}\right\}d\xi. \tag{3}$$

In the case of *in vitro* experiments, we have $r_{\rm c}, r_{\rm ai}$, and $r_{\rm ao}$ much larger than $h_{\rm SC}$ and $h_{\rm D}$. Thus, equation (2) can be simplified as

$$|Z|\approx\frac{2\chi}{\pi\left(\varepsilon_{\rm D}h_{\rm D}+\varepsilon_{\rm SC}h_{\rm SC}\right)}\cdot\left[Z_3\left(\frac{r_{\rm ao}}{r_{\rm c}},\frac{r_{\rm ai}}{r_{\rm c}}\right)+Z_1\left(\frac{r_{\rm ao}}{r_{\rm c}},\frac{r_{\rm ai}}{r_{\rm c}}\right)\frac{\varepsilon_{\rm D}h_{\rm D}h_{\rm SC}}{\varepsilon_{\rm SC}r_{\rm c}^2}\right] \tag{4}$$

where r_c is radius of inner circular electrode, r_{ai} and r_{ao} the inner and outer radii of outer annulus electrodes, h_{SC} and h_D the depths of the SC and deep tissue layer, ε_{SC} and ε_D the permittivity of SC and deep tissue layer, respectively. In addition, $\chi = (\sigma_{SC}^2/\varepsilon_{SC}^2 + 4\pi^2 f^2)^{-1/2}$ and the nondimensional functions Z_3 and Z_1 are given by

$$Z_m(a,b) = \int_0^\infty \left[J_1(\eta) - \frac{aJ_1(a\eta) - bJ_1(b\eta)}{a^2 - b^2} \right]^2 \frac{d\eta}{\eta^m} \quad (5)$$

where f is the frequency conducted in the measurements, J_1 is the Bessel function of the first kind. Equation (4) analytically gives the dependence of impendence on all material parameters, thicknesses, geometry, and frequency.

For *in vivo* experiments that involve a thick deep tissue layer, i.e., $h_D \gg h_{SC}$, the impedance can then be written as

$$|Z| \approx \frac{2\chi}{\pi \varepsilon_{SC} r_c} \left\{ \begin{array}{l} \left(1 - \dfrac{\varepsilon_{SC}^2}{\varepsilon_D^2}\right) \dfrac{h_{SC}}{r_c} \left[Z_1\left(\dfrac{r_{ao}}{r_c}, \dfrac{r_{ai}}{r_c}\right) \right. \\ \quad \left. - Y\left(\dfrac{r_{ao}}{r_c}, \dfrac{r_{ai}}{r_c}, \dfrac{\varepsilon_D r_c}{\varepsilon_{SC} h_{SC}}\right) \right] \\ \quad + \dfrac{\varepsilon_{SC}}{\varepsilon_D} Z_2\left(\dfrac{r_{ao}}{r_c}, \dfrac{r_{ai}}{r_c}\right) \end{array} \right\} \quad (6)$$

where Z_1 and Z_2 are given in (5) and

$$Y(a,b,c) = \int_0^\infty \left[J_1(\eta) - \frac{aJ_1(a\eta) - bJ_1(b\eta)}{a^2 - b^2} \right]^2 \frac{d\eta}{\eta + c}. \quad (7)$$

The permittivity of the SC and deep tissue layer decreases as the frequency increases and the opposite holds for the conductivity [63]. For frequencies between 15 kHz to 1.25 MHz, $\varepsilon_{SC}/\varepsilon_0$ and $\varepsilon_D/\varepsilon_0$ decrease from 1.47×10^3 and 3.79×10^2 to 7.48×10^4 and 2.34×10^3, respectively, whereas σ_{SC} increases from 1.62×10^{-4} to 1.97×10^{-2} S/m. For electrodes with $r_c = 100$ μm, $r_{ai} = 300$ μm, $r_{ao} = 400$ μm, and for $h_{SC} = 20$ μm, the modeling result of the frequency dependence of the sensor impedance shown in Fig. 6(a) indicates that the sensor impedance decreases consistently with hydration levels at all simulated frequencies between 15 kHz to 1.25 MHz. The result also indicates that the sensor has higher sensitivity at lower measurement frequencies, which is consistent with the experimental data. As shown in Fig. 6(b), the impedance in (3) versus the chamber height h_D agrees well with the *in vitro* experiments (shown in the same figure) for an interfacial capacitance of 0.25 [64] at frequencies varied from 15 kHz to 1.25 MHz. The geometry dependence of the sensor impedance at various frequencies appears in Fig. 6(c), in which the sensor impedance decreases monotonously with decreasing electrode spacing ($h_{SC} = 20$ μm, $r_{ai} = 300$ μm, $r_{ao} = 400$ μm, and varying r_c). When r_c increases from 60 to 200 μm, the impedance decreases by 29.6%, agreeing well with the *in vitro* experimental data shown also in Fig. 6(c). In addition, both the measurement frequencies and the sensor geometry influence the effective measurement depths of the sensor (see Fig. 6(b)–(d)], in a manner consistent with experiments. The effective measurement depths ($h_D + h_{SC}$) of the sensor are close to 50 μm at 15 kHz at $r_c = 60$ μm; at r_c of 180 μm, the effective depth is greater than 80 μm, again compatible with *in vitro* studies. The simulated results indicate that the measurement frequency and sensor geometry can both affect sensor impedance and the effective measurement depths. Measurements of hydration levels at different skin depths, therefore, can be achieved by adjusting the frequency and geometry.

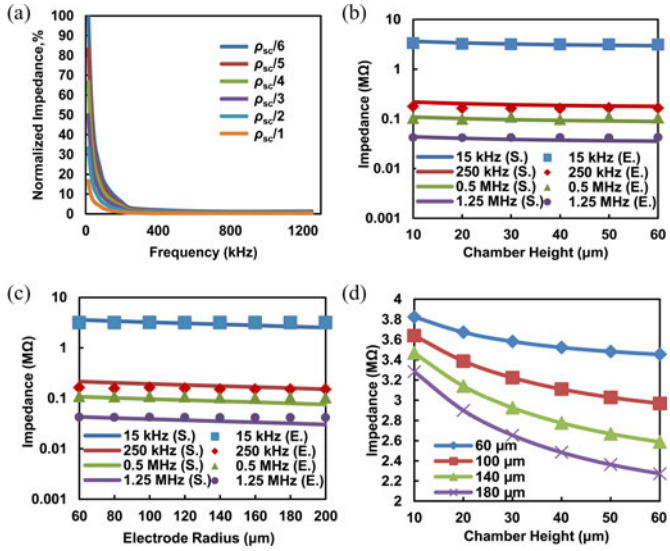

Fig. 6. (a) Simulated sensor impedance as a function of hydration (indicated by different levels of ρ_{sc}) at frequencies from 15 kHz to 1.25 MHz. (b) Simulated sensor impedance (labeled with S.) of as a function of chamber heights at frequencies from 15 kHz to 1.25 MHz, with comparison to *in vitro* experimental results (labeled with E.). (c) Simulated sensor impedance (labeled with S.) as a function of electrode spacing at frequencies from 15 kHz to 1.25 MHz and a chamber height of 30 μm, with comparison to *in vitro* experimental results (labeled with E.). (d) Simulated sensor impedance as a function of chamber height for electrode radii between 60 to 180 μm, at a frequency of 15 kHz.

E. Responses of Depth Profiling Hydration Sensors to Hydration Changes

In vivo measurements involve evaluations at a fixed frequency of 15 kHz, where the impedance depends strongly on hydration levels and the electrode spacing controls the measurement depth. As illustrated in Fig. 7(a)–(c), the impedance varies systematically with electrode spacing and with hydration levels. For example, at a fixed hydration level of 47.8, the impedance decreases consistently with the radii of the inner circular electrodes r_c from 1.7 to 0.25 MΩ when r_c varies from 60 to 200 μm in Fig. 7(c), indicating a strong expected geometry dependence. In addition, as the hydration level decreases from 96 [see Fig. 7(a)] to 47.8 [Fig. 7(c)], the differences between impedances measured using electrodes with r_c of 60 μm and 200 μm diminish, suggesting that the effect of geometry dependence is more prominent at low hydration levels. Fig. 7(d) shows that the hydration determined by CHS changes from 64 to 114 shortly after the application of lotion, and then decreases back to 56 over the next ~35 min. Sensors with electrodes that have r_c of 60 and 140 μm follow the same trend. By contrast, electrodes with r_c of 200 μm reveal an initial impedance that is larger than the final impedance, indicating that the hydration levels measured by these electrodes are higher than the original values.

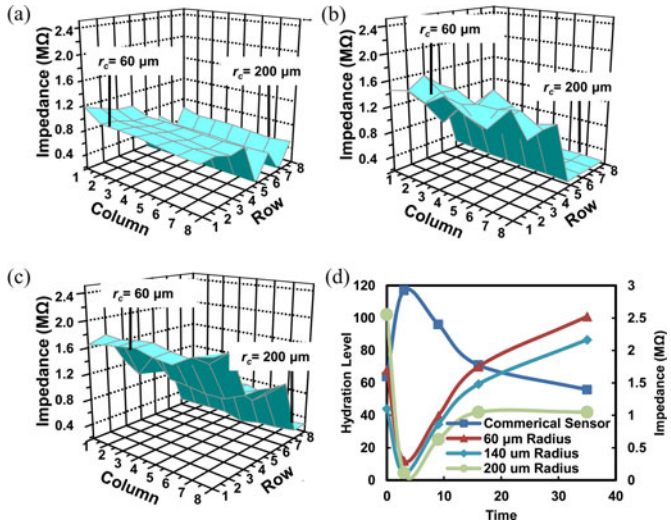

Fig. 7. Measurement results obtained with a depth profiling epidermal hydration sensor operating at a frequency of 15 kHz, for hydration levels of (a) 96, (b) 63, and (c) 47.8 when the radii of the inner circular electrodes (r_c) changes from 60 to 200 μm. (d) Impedance of selected electrodes at 15 kHz with comparison to results from a commercial sensor.

These results are consistent with the *in vitro* experiments; they suggest that electrodes with r_c of 60 and 140 μm follow the hydration levels in the SC, while electrodes with r_c of 200 μm may partially capture the hydration levels below the SC, where the improvement of the barrier function of the SC after applying the lotion could increase the hydration level by minimizing the rate of TEWL.

F. Skin Hydration Imaging

In multiplexed array formats, epidermal hydration sensors can reveal spatial gradients in hydration across the surface of the skin. As a demonstration, variations in hydration level are intentionally created through application of lotion in horizontal and vertical lines. The skin absorbs the lotion, to change the hydration level in the skin itself. Spatial patterns in the application of lotion create corresponding spatial variations in hydration, thereby providing situations similar to those during transdermal drug delivery [65], atopic eczema [66], and wound and burn healing processes [67], in which hydration levels in the skin are nonuniform. To minimize the variations of impedance between electrodes due to skin contours, experimental results are shown as relative impedance changes (see Fig. 8) obtained by subtracting impedance values measured prior to and 1 min after applying the lotion. The average impedance decrease over most of the area is $\sim$1.9 MΩ, indicating large increases in hydration. Areas that are free of lotion show impedance changes of $\sim$0.2 MΩ, consistent with expected minimal changes in hydration. Regions between lines of applied lotion [see Fig. 8(b)] exhibit impedance changes of $\sim$1.2 MΩ, perhaps due to some lateral diffusion of the lotion. A result using depth profiling devices with layouts of Fig. 1(c) also reveals impedance changes consistent with the patterns of lotion [see Fig. 8(c)]. Here, the overall impedance increases from top to bottom, as expected based on differences in electrode geometries. Some nonsystematic variations are also observed, due to likely nonuniformities of the skin itself. As any endogenous and exogenous patterns on the skin can potentially change the localized skin hydration due to underlying changes of water barrier function. The ability of the hydration mapping sensor to identify spatial gradients in hydration indicates a capacity for recognizing these invisible patterns.

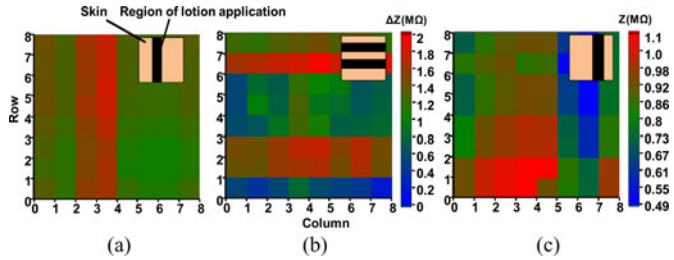

Fig. 8. Demonstration of depth profiling and spatial mapping with epidermal devices. Lotion was selectively applied to the skin in patterned geometries (illustrations in the insets) of (a) a vertical line, (b) two horizontal lines, and (c) a vertical line.

V. Conclusion

The sensor technology introduced here provides a soft, "skin-like" device that can integrate with the skin intimately and noninvasively to quantify the regional hydration levels. The spatial sensitivity and ability to monitor large areas can be achieved by scaling the electrode spacing and number, in a straightforward manner that requires no significant changes in sensor design measurement setups. Epidermal impedance mapping devices provide appealing means to monitor biophysical signals over large areas. The data acquisition electronics can be reduced in size [40] and, potentially, be integrated into the epidermal platform itself. Also, stretching, bending, and other mechanical deformations can alter the capacitance of the electrode pairs, in a manner that could affect the assessment of hydration. One possible solution involves a differential measurement mechanism based on an additional pair of reference electrodes that are decoupled from the skin but located adjacent to the sensing electrodes.

References

[1] K. R. Feingold, "The outer frontier: The importance of lipid metabolism in the skin," *J. Lipid. Res.*, vol. 50, pp. S417–S22, 2009.

[2] S. P. Song, C. Z. Lv, K. R. Feingold, Q. N. Hou, Z. Y. Li, C. Y. Guo, P. M. Elias, and M. Q. Man, "Abnormalities in stratum corneum function in patients recovered from leprosy," *Skin Pharmacol. Physiol.*, vol. 22, pp. 131–6, 2009.

[3] F. M. Hendriks, D. Brokken, C. W. J. Oomens, and F. P. T. Baaijens, "Influence of hydration and experimental length scale on the mechanical response of human skin in vivo, using optical coherence tomography," *Skin. Res. Technol.*, vol. 10, pp. 231–41, 2004.

[4] S. Sasai, Y.-X. Zhen, and H. Tagami, "High-frequency conductance measurement of the skin surface hydration state of dry skin using a new probe studded with needle-form electrodes (MT-8 C)," *Skin. Res. Technol.*, vol. 2, pp. 173–6, 1996.

[5] B. Eberlein-Konig, T. Schafer, J. Huss-Marp, U. Darsow, M. Mohrenschlager, O. Herbert, D. Abeck, U. Kramer, H. Behrendt, and J. Ring, "Skin surface pH, stratum corneum hydration, trans-epidermal water loss and skin roughness related to atopic eczema and skin dryness in

a population of primary school children," *Acta Derm. Venereol.*, vol. 80, pp. 188–91, 2000.

[6] J. Gupta, E. Grube, M. B. Ericksen, M. D. Stevenson, A. W. Lucky, A. P. Sheth, A. H. Assa'ad, and G. K. Khurana Hershey, "Intrinsically defective skin barrier function in children with atopic dermatitis correlates with disease severity," *J. Allergy Clin. Immunol.*, vol. 121, pp. 725.e2–730.e2, 2008.

[7] K. L. Hon, K. Y. Wong, T. F. Leung, C. M. Chow, and P. C. Ng, "Comparison of skin hydration evaluation sites and correlations among skin hydration, transepidermal water loss, SCORAD index, Nottingham Eczema severity score, and quality of life in patients with atopic dermatitis," *Am. J. Clin. Dermatol.*, vol. 9, pp. 45–50, 2008.

[8] S. D. Kim, C. H. Huh, K. I. Seo, D. H. Suh, and J. I. Youn, "Evaluation of skin surface hydration in Korean psoriasis patients: A possible factor influencing psoriasis," *Clin. Exp. Dermatol.*, vol. 27, pp. 147–52, 2002.

[9] C. Blichmann and J. Serup, "Hydration studies on scaly hand eczema," *Contact Dermatitis*, vol. 16, pp. 155–9, 1987.

[10] B. Cravello and A. Ferri, "Relationships between skin properties and environmental parameters," *Skin. Res. Technol.*, vol. 14, pp. 180–6, 2008.

[11] J. W. Choi, S. H. Kwon, C. H. Huh, K. C. Park, and S. W. Youn, "The influences of skin visco-elasticity, hydration level and aging on the formation of wrinkles: A comprehensive and objective approach," *Skin. Res. Technol.*, pp. 1–7, 2012.

[12] B. W. Tran, A. D. Papoiu, C. V. Russoniello, H. Wang, T. S. Patel, Y. H. Chan, and G. Yosipovitch, "Effect of itch, scratching and mental stress on autonomic nervous system function in atopic dermatitis," *Acta. Derm. Venereol.*, vol. 90, pp. 354–61, 2010.

[13] P. G. Sator, J. B. Schmidt, T. Rabe, and C. C. Zouboulis, "Skin aging and sex hormones in women—Clinical perspectives for intervention by hormone replacement therapy," *Exp. Dermatol.*, vol. 13, no. suppl. 4, pp. 36–40, 2004.

[14] M. Boguniewicz, N. Nicol, K. Kelsay, and D. Y. M. Leung, "A multidisciplinary approach to evaluation and treatment of atopic dermatitis," *Semin. Cutan. Med. Surg.*, vol. 27, pp. 115–27, 2008.

[15] V. M. Sharma, K. Sridharan, G. Pichan, and M. R. Panwar, "Influence of heat-stress induced dehydration on mental functions," *Ergonomics*, vol. 29, pp. 791–9, 1986.

[16] S. M. Kleiner, "Water: An essential but overlooked nutrient," *J. Am. Diet. Assoc.*, vol. 99, pp. 200–6, 1999.

[17] S. Verdier-Sévrain and F. Bonté, "Skin hydration: A review on its molecular mechanisms," *J. Cosmetic. Dermatol.*, vol. 6, pp. 75–82, 2007.

[18] M. Zhang and A. F. T. Mak, "In vivo friction properties of human skin," *Prosthet. Orthot. Int.*, vol. 23, pp. 135–41, 1999.

[19] J. W. Choi, S. H. Kwon, C. H. Huh, K. C. Park, and S. W. Youn, "The influences of skin visco-elasticity, hydration level and aging on the formation of wrinkles: A comprehensive and objective approach," *Skin. Res. Technol.*, vol. 19, pp. 1–7, 2012.

[20] L.-C. Gerhardt, V. Strässle, A. Lenz, N. D. Spencer, and S. Derler, "Influence of epidermal hydration on the friction of human skin against textiles," *J. R. Soc. Interface.*, vol. 5, pp. 1317–28, 2008.

[21] H. Tagami, M. Ohi, K. Iwatsuki, Y. Kanamaru, M. Yamada, and B. Ichijo, "Evaluation of the skin surface hydration in vivo by electrical measurement," *J. Investig. Dermatol.*, vol. 75, pp. 500–7, 1980.

[22] M. Paye, D. Van de Gaer, and B. M. Morrison, "Corneometiy measurements to evaluate skin dryness in the modified soap chamber test," *Skin. Res. Technol.*, vol. 1, pp. 123–7, 1995.

[23] P. Xiao, L. I. Ciortea, H. Singh, Y. Cui, E. P. Berg, and R. E. Imhof, "Optothermal in-vivo skin hydration measurements—A comparison study of different measurement techniques," in *J. Phys.: Conf. Ser.*, 2010, vol. 214, p. 012026.

[24] T. Frodin, P. Helander, L. Molin, and M. Skogh, "Hydration of human stratum corneum studied in vivo by optothermal infrared spectrometry, electrical capacitance measurement, and evaporimetry," *Acta. Derm. Venereol.*, vol. 68, pp. 461–7, 1988.

[25] E. M. Attas, M. G. Sowa, T. B. Posthumus, B. J. Schattka, H. H. Mantsch, and S. L. Zhang, "Near-IR spectroscopic imaging for skin hydration: The long and the short of it," *Biopolymers*, vol. 67, pp. 96–106, 2002.

[26] F. Kadlec, M. Berta, P. Kužel, F. Lopot, and V. Polakovič, "Assessing skin hydration status in haemodialysis patients using terahertz spectroscopy: A pilot/feasibility study," *Phys. Med. Biol.*, vol. 53, pp. 7063–71, 2008.

[27] F. M. Hendriks, *Mechanical Behaviour of Human Epidermal and Dermal Layers In Vivo*.Technische Universiteit Eindhoven, Eindhoven, The Netherlands: Technische Universiteit Eindhoven, 2005.

[28] G. Tan, P. Xu, L. B. Lawson, J. He, L. C. Freytag, J. D. Clements, and V. T. John, "Hydration effects on skin microstructure as probed by high-resolution cryo-scanning electron microscopy and mechanistic implications to enhanced transcutaneous delivery of biomacromolecules," *J. Pharm. Sci.*, vol. 99, pp. 730–40, 2010.

[29] E. Alanen, J. Nuutinen, K. Nicklén, T. Lahtinen, and J. Mönkkönen, "Measurement of hydration in the stratum corneum with the MoistureMeter and comparison with the Corneometer," *Skin. Res. Technol.*, vol. 10, pp. 32–7, 2004.

[30] J. W. Fluhr, M. Gloor, S. Lazzerini, P. Kleesz, R. Grieshaber, and E. Berardesca, "Comparative study of five instruments measuring stratum corneum hydration (Corneometer CM 820 and CM 825, Skicon 200, Nova DPM 9003, DermaLab)—Part I: *In vitro*," *Skin. Res. Technol.*, vol. 5, pp. 161–70, 1999.

[31] A. O. Barel and P. Clarys, "In vitro calibration of the capacitance method (Corneometer CM 825) and conductance method (Skicon-200) for the evaluation of the hydration state of the skin," *Skin. Res. Technol.*, vol. 3, pp. 107–13, 1997.

[32] P. Clarys, A. O. Barel, and B. Gabard, "Non-invasive electrical measurements for the evaluation of the hydration state of the skin: comparison between three conventional instruments—the Comeometer®, the Skicon® and the Nova DPM®," *Skin. Res. Technol.*, vol. 5, pp. 14–20, 1999.

[33] J. L. Lévêque and B. Querleux, "SkinChip®, a new tool for investigating the skin surface in vivo," *Skin. Res. Technol.*, vol. 9, pp. 343–7, 2003.

[34] D. Batisse, F. Giron, and J. L. Que, "Capacitance imaging of the skin surface," *Skin. Res. Technol.*, vol. 12, pp. 99–104, 2006.

[35] E. Uhoda, J. L. Lévêque, and G. E. Piérarda, "Silicon image sensor technology for in vivo detection of surfactant-induced corneocyte swelling and drying," *Dermatology*, vol. 210, pp. 184–8, 2005.

[36] E. Alanen, T. Lahtinen, and J. Nuutinen, "Variational formulation of open-ended coaxial line in contact with layered biological medium," *IEEE Trans. Biomed. Eng.*, vol. 45, pp. 1241–8, 1998.

[37] T. J. Ryan, M. Thoolen, and Y. H. Yang, "The effect of mechanical forces (vibration or external compression) on the dermal water content of the upper dermis and epidermis, assessed by high frequency ultrasound," *J. Tissue Viability*, vol. 11, pp. 97–101, 2001.

[38] C. G. Rylander, T. E. Milner, S. A. Baranov, and J. S. Nelson, "Mechanical tissue optical clearing devices: Enhancement of light penetration in ex vivo porcine skin and adipose tissue," *Laser Surg. Med.*, vol. 40, pp. 688–94, 2008.

[39] A. A. Gurjarpadhye, W. C. Vogt, Y. Liu, and C. G. Rylander, "Effect of localized mechanical indentation on skin water content evaluated using OCT," *Int. J. Biomed. Imag*, vol. 2011, p. 817250, 2011.

[40] X. Huang, W.-H. Yeo, Y. Liu, and J. Rogers, "Epidermal differential impedance sensor for conformal skin hydration monitoring," *Biointerphases*, vol. 7, pp. 1–9, 2012.

[41] Ø. G. Martinsen, S. Grimnes, and E. Haug, "Measuring depth depends on frequency in electrical skin impedance measurements," *Skin. Res. Technol.*, vol. 5, pp. 179–81, 1999.

[42] M. S. Kim, Y. Cho, S. T. Seo, C. S. Son, H. J. Park, and Y. N. Kim, "A new method for non-invasive measurement of skin in the low frequency range," *Healthc Inf. Res.*, vol. 16, pp. 143–8.

[43] A. O. Barel and P. Clarys ,*Handbook of Non-Invasive Methods and the Skin*, Boca Raton, FL: CRC Press, pp. 337–44.

[44] T. Yamamoto and Y. Yamamoto, "Electrical properties of the epidermal stratum corneum," *Med. Biol. Eng. Comput.*, vol. 14, pp. 151–8, 1976.

[45] D.-H. Kim, N. Lu, R. Ma, Y.-S. Kim, R.-H. Kim, S. Wang, J. Wu, S. M. Won, H. Tao, A. Islam, K. J. Yu, T.-I. Kim, R. Chowdhury, M. Ying, L. Xu, M. Li, H.-J. Chung, H. Keum, M. McCormick, Liu P., Y.-W. Zhang, F. G. Omenetto, Y. Huang, T. Coleman, and J. A. Rogers, "Epidermal electronics," *Science*, vol. 333, pp. 838–43, 2011.

[46] E. J. Clar, C. P. Her, and C. G. Sturelle, "Skin impedance and moisturization," *J. Soc. Cosmetic Chemists*, vol. 26, pp. 337–53, 1975.

[47] G. McKeen and M. Lindinger, "Prediction of hydration status using multi-frequency bioelectrical impedance analysis during exercise and recovery in horses," *Equine Comp. Exerc. Physiol.*, vol. 1, pp. 199–209, 2004.

[48] H. Scharfetter, P. Brunner, M. Mayer, B. Brandstatter, and H. Hinghofer-Szalkay, "Fat and hydration monitoring by abdominal bioimpedance analysis: Data interpretation by hierarchical electrical modeling," *IEEE Trans. Biomed. Eng.*, vol. 52, no. 6, pp. 975–82, Jun. 2005.

[49] B. Esler, T. Lyons, S. Turovets, and D. Tucker, "Instrumentation for low frequency EIT studies of the human head and its validation in phantom experiments,"," in *J. Phys.: Conf. Ser.*, 2010, vol. 224, p. 012007.

[50] K. Ito, K. Furuya, Y. Okano, and L. Hamada, "Development and characteristics of a biological tissue-equivalent phantom for microwaves," *Electron. Commun. Jpn. (Part I: Communications)*, vol. 84, pp. 67–77, 2001.

[51] G. Pellacani and S. Seidenari, "Water sorption-desorption test and moisture accumulation test for functional assessment of atopic skin in children," *Acta Derm. Venereol.*, vol. 81, pp. 100–3, 2001.

[52] D van Neste, "*In vivo* evaluation of unbound water accumulation in stratum corneum. The influence of acute skin irritation induced by sodium laurylsulfate," *Dermatologica*, vol. 181, pp. 197–201, 1990.

[53] T. Zioni, N. Perkas, Y. Wolfus, Y. Soroka, I. Popov, M. Oron, I. Perelshtein, Y. Bruckental, F. M. Brégégère, Z. Ma'or, A. Gedanken, Y. Yeshurun, R. Neuman, and Y. Milner, "Strontium hexaferrite nanomagnets suspended in a cosmetic preparation: A convenient tool to evaluate the biological effects of surface magnetism on human skin," *Skin. Res. Technol.*, vol. 16, pp. 316–24, 2010.

[54] V. R. Leite e Silva, M. A. Schulman, C. Ferelli, J. M. Gimenis, G. W. Ruas, A. R. Baby, M. V. Velasco, M. E. Taqueda, and T. M. Kaneko, "Hydrating effects of moisturizer active compounds incorporated into hydrogels: In vivo assessment and comparison between devices," *J. Cosmet. Dermatol.*, vol. 8, pp. 32–9, 2009.

[55] H. N. Mayrovitz, M. Bernal, F. Brlit, and R. Desfor, "Biophysical measures of skin tissue water: Variations within and among anatomical sites and correlations between measures," *Skin. Res. Technol.*, vol. 19, pp. 47–54, 2013.

[56] E. Cronin and R. B. Stoughton, "Regional variations and the effect of hydration and epidermal stripping," *Brit. J. Dermatol.*, vol. 74, pp. 265–72, 1962.

[57] C. Gabriel, S. Gabriel, and E. Corthout, "The dielectric properties of biological tissues—Part I: Literature survey," *Phys. Med. Biol.*, vol. 41, pp. 2231–49, 1996.

[58] C. Gabriel, A. Peyman, and E. H. Grant, "Electrical conductivity of tissue at frequencies below 1 MHz," *Phys. Med. Biol.*, vol. 54, pp. 4863–78, 2009.

[59] T. Sunaga, H. Ikehira, S. Furukawa, H. Shinkai, H. Kobayashi, Y. Matsumoto, E. Yoshitome, T. Obata, S. Tanada, H. Murata, and Y. Sasaki, "Measurement of the electrical properties of human skin and the variation among subjects with certain skin conditions," *Phys. Med. Biol.*, vol. 47, pp. N11–N5, 2002.

[60] V. Raicu, N. Kitagawa, and A. Irimajiri, "A quantitative approach to the dielectric properties of the skin," *Phys. Med. Biol.*, vol. 45, pp. L1–L4, 2000.

[61] J. L. Leveque and J. D. Rigal, "Impedance methods for studying skin moisturization," *J. Cosmet. Sci.*, vol. 34, pp. 419–28, 1983.

[62] A. E. Siegman, "Quasi fast Hankel transform," *Opt. Lett.*, vol. 1, pp. 13–5, 1977.

[63] T. Yamamoto and Y. Yamamoto, "Electrical properties of the epidermal stratum corneum," *Med. Biol. Eng.*, vol. 14, pp. 151–8, 1976.

[64] R. M. Williams, M. E. Loveland, B. Jeffries-Nakamura, M. L. Underwood, C. P. Bankston, H. Leduc, and J. T. Kummer, "Kinetics and transport at AMTEC electrodes," *J. Electrochem. Soc.*, vol. 137, pp. 1709–16, 1990.

[65] H. A. Benson, "Transdermal drug delivery: Penetration enhancement techniques," *Curr. Drug Del.*, vol. 2, pp. 23–33, 2005.

[66] E. A. Holm, H. C. Wulf, L. Thomassen, and G. B. E. Jemec, "Instrumental assessment of atopic eczema: Validation of transepidermal water loss, stratum corneum hydration, erythema, scaling, and edema," *J Amer. Acad. Dermatol.*, vol. 55, pp. 772–80, 2006.

[67] C.-C. Chang, Y.-F. Kuo, H.-C. Chiu, J.-L. Lee, T.-W. Wong, and S.-H. Jee, "Hydration, not silicone, modulates the effects of keratinocytes on fibroblasts," *J. Surg. Res.*, vol. 59, pp. 705–11, 1995.

Authors' photographs and biographies not available at the time of publication.